Electronic Supplementary Material (ESI) for CrystEngComm.

Supporting Information

A new multifunctional anionic 3D Zn(II)-MOF based on heptanuclear clusters: selective adsorption of organic dyes and dual-emitting sensor for nitroantibiotics

Yan-Fang Du[a], Xi-Xi Wang[a], Ai-Ling Cheng*[a], Yuan-Yuan Wang[a], En-Qing Gao[b]

[a] *College of Chemistry and Molecular Engineering, East China Normal University, Shanghai 200240, People's Republic of China.*

[b] *Shanghai Key Laboratory of Green Chemistry and Chemical Processes, College of Chemistry and Molecular Engineering, East China Normal University, Shanghai 200062, People's Republic of China.*

Contents

S1. General methods

Powder X-ray diffraction (PXRD) patterns were collected on a Rigaku ULTIMA IV diffractometer equipped with Cu Kα in a 2θ range of 5–40°. FT-IR spectra were recorded on a Nicolet NEXUS 670 spectrophotometer using KBr pellets in the range of 500–4000 cm^{-1}. Elemental analyses (C, H and N) were performed on an Elementar Vario ELIII analyzer. Inductively coupled plasma (ICP) experiment was conducted with a ThermoFisher ICAP7200HS emission spectrometer. TG analyses were carried out on a Mettler Toledo TGA/SDTA851 instrument under flowing N_2 or air atmosphere with a heating rate of 5°C min^{-1}. UV-visible absorption spectra were measured on a SHIMADZU UV-1800 spectrophotometer. Fluorescence spectra were recorded at room temperature with an Edinburgh FLS980 fluorescence spectrophotometer. The zeta potential was performed by JS94H microiontophoresis apparatus.

S2. X-ray Crystallography.

Diffraction intensity data for **1** was collected on a Bruker Apex II CCD area detector equipped with graphite-monochromated Mo-Kα radiation (λ = 0.71073 Å) at 293K. Empirical absorption correction was applied using the SADABS program. The structure was solved by direct methods and refined by the full-matrix least-squares based on F^2 using SHELXTL. The non-hydrogen atoms were refined anisotropically, and the hydrogen atoms of the ligands were placed in calculated positions and refined using a riding model. Notably, the solvent molecules are highly disordered and could not be modeled correctly, so the residual electron densities resulting from them were removed by Solvent Mask in Olex2. A solvent mask was calculated and 2424 electrons were found in a volume of 17477Å3 in 1 void per unit cell. This is consistent with the presence of 1 $[C2H8N]^+$, 6[C_2H_9NO] and 24[H_2O] per Formula Unit which account for 2412 electrons per unit cell.

S3. Explanation for the Alert A and B in the CheckCIF reports

Alert level B

PLAT241_ALERT_2_B High 'MainMol' Ueq as Compared to Neighbors of O1 Check

Explanation: This alert comes from the large amount of disorder in the structure and the poor quality of the crystal data.

Table S1. Crystal data and structural refinements for **1**.

Complex	**CP-1**
Formula	$Zn_7C_{116}H_{163}O_{76}N_7S_6$
Fw	3521.65
Crystal system	trigonal
Space group	$R\bar{3}c$
a (Å)	20.7129(8)
b (Å)	20.7129(8)
c (Å)	77.627(3)
α	90
β	90
γ	120
V (Å^3)	28842.1(18)
Z	6
ρ_{calc} (g m^{-3})	1.178
μ (mm^{-1})	2.224
F(000)	10616.064
reflections collected	104521
unique reflections	6539
R_{int}	0.0768
GOF	1.0035
R_1 [I>2σ(I)]	0.0862
wR_2 (all data)	0.3089

*The refinement results were obtained from Olex2 using Solvent Mask.

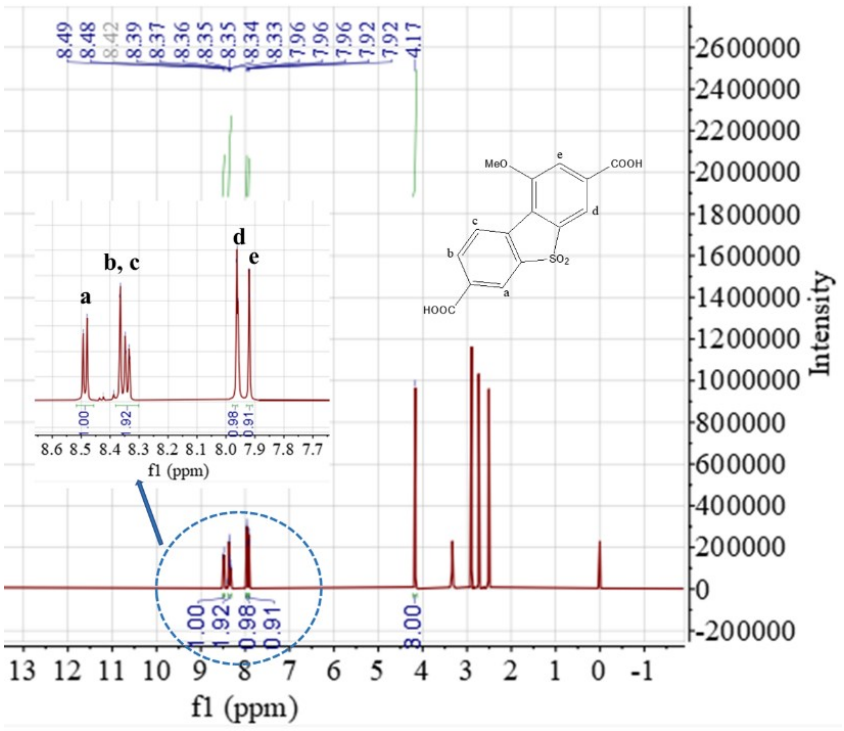

Figure S1. ^{1}H-NMR (DMSO-d6, 500 MHz) spectrum of H_2L. δ: 4.13 (s, 3H, -OCH3), 7.87 (1H), 7.93 (1H), 8.2-8.5 (3H).

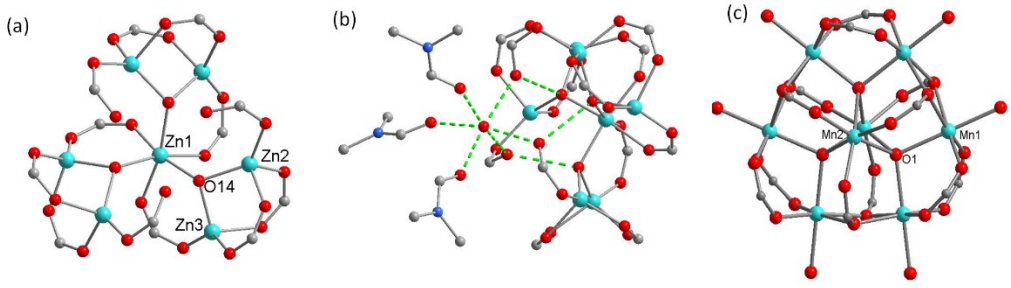

Figure S2. $[Zn_7(\mu_3\text{-}OH)_3(COO)_6]$ SBU of UoC-1 (a and b); $[Mn_8(\mu_4\text{-}O)_3(COO)_{12}]$ SBU of Mn-1 (c).

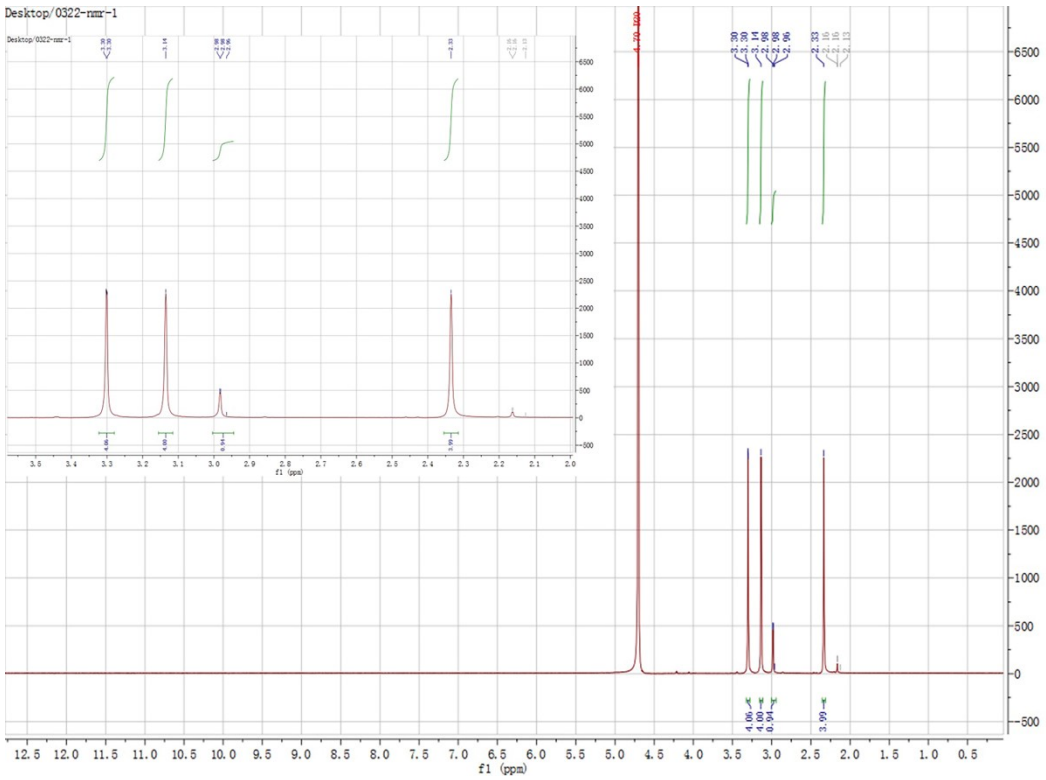

Figure S3. ^{1}H-NMR (D_2O) spectrum of the NaCl solution after soaking **1**. (DMA molecules also release from the framework owing to the partial collapse of **1** in water.) δ: 2.33 (-OC-CH_3), 2.98(-N-CH_3), 3.14 (-CO-N-CH_3), 3.30 (-CO-N-CH_3).

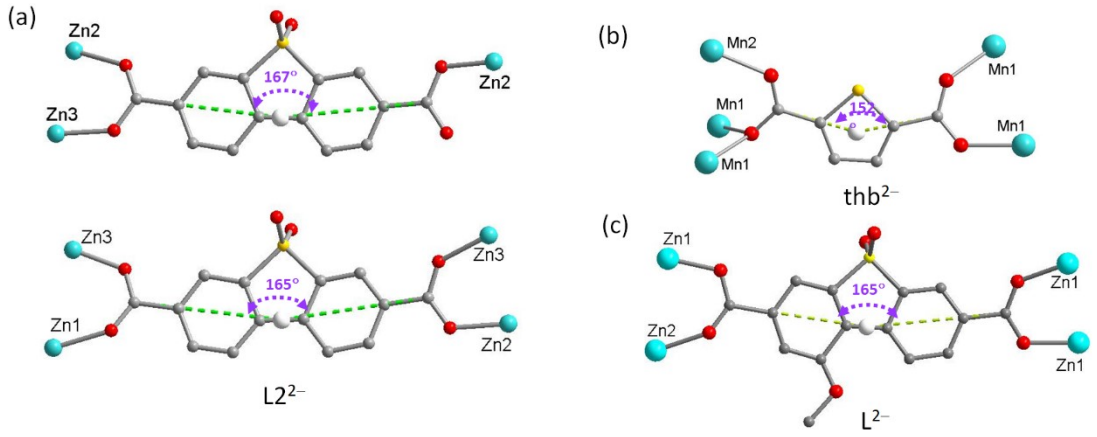

Figure S4. Coordination environment of the ligand in UoC-1 (a), Mn-MOF (b) and **1** (c).

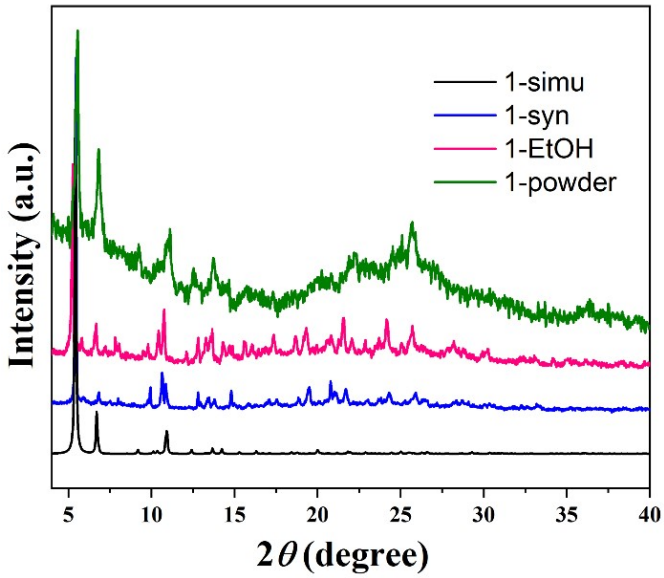

Figure S5. PXRD patterns showing the purity and stability of **1**.

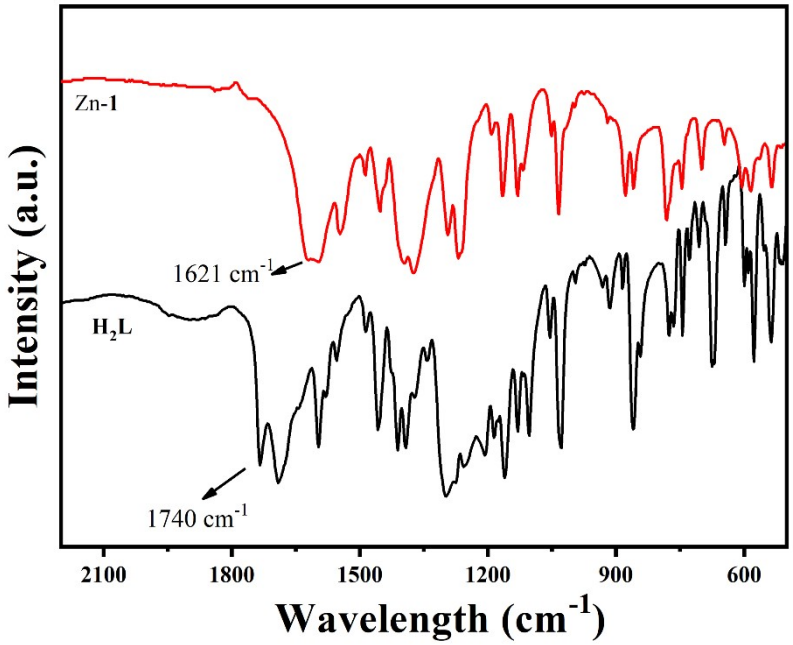

Figure S6. IR spectra of H_2L ligand and complex **1**.

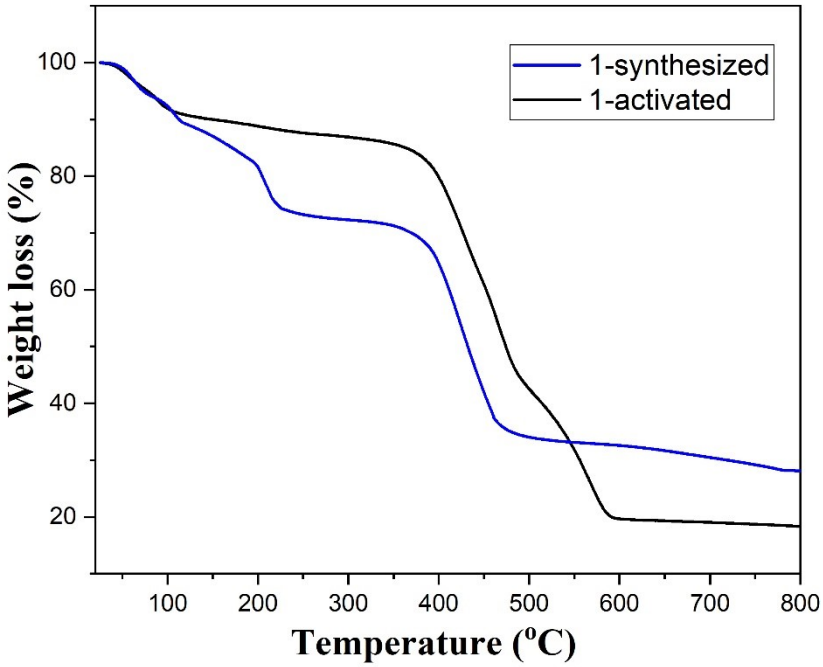

Figure S7. TGA curves of the as-synthesized **1** (under N_2 atmosphere) and the activated samples of **1** (under air). The evacuated sample of **1** was obtained by solvent exchange with EtOH for three days, during which time the solvent was changed every 12 hours, then dried under vacuum at 180°C for 12 hours.

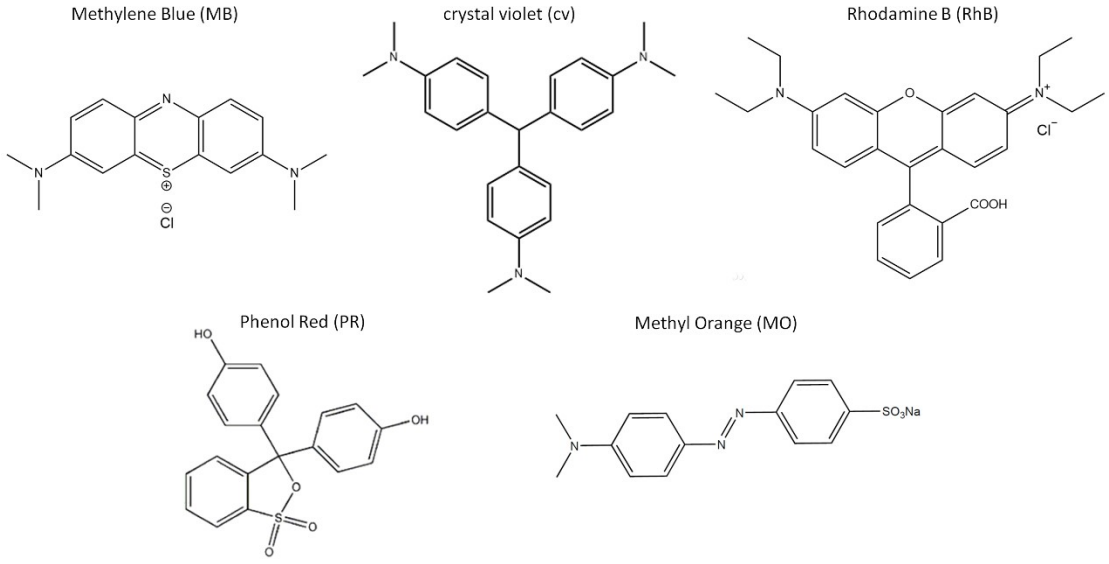

Figure S8. Molecular structures of the organic dye compounds.

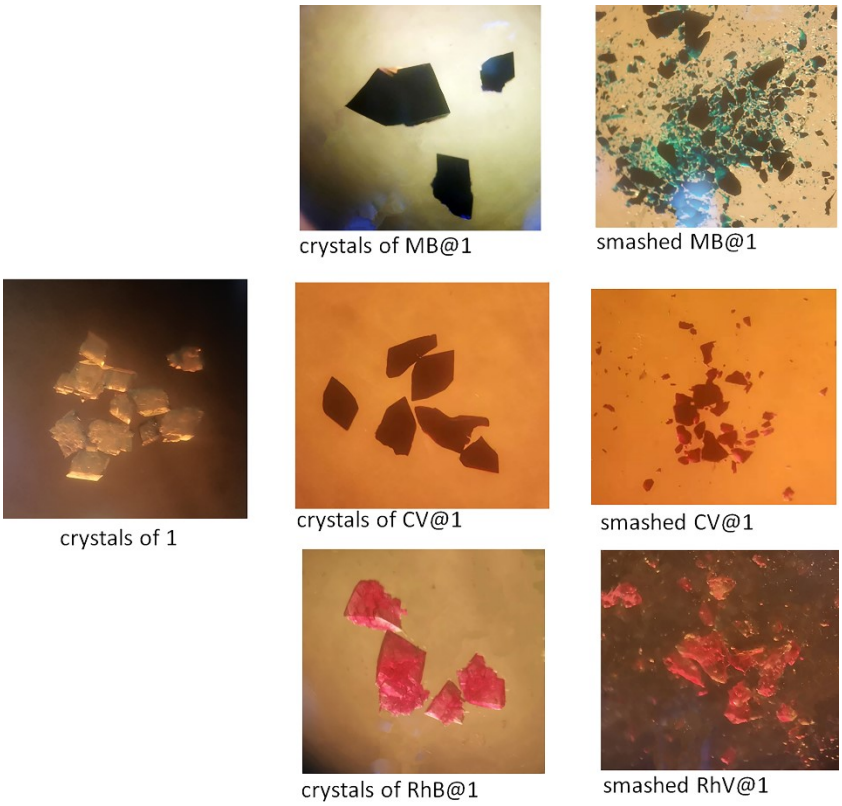

Figure S9. Photographs of crystal samples of **1** and dye@**1**.

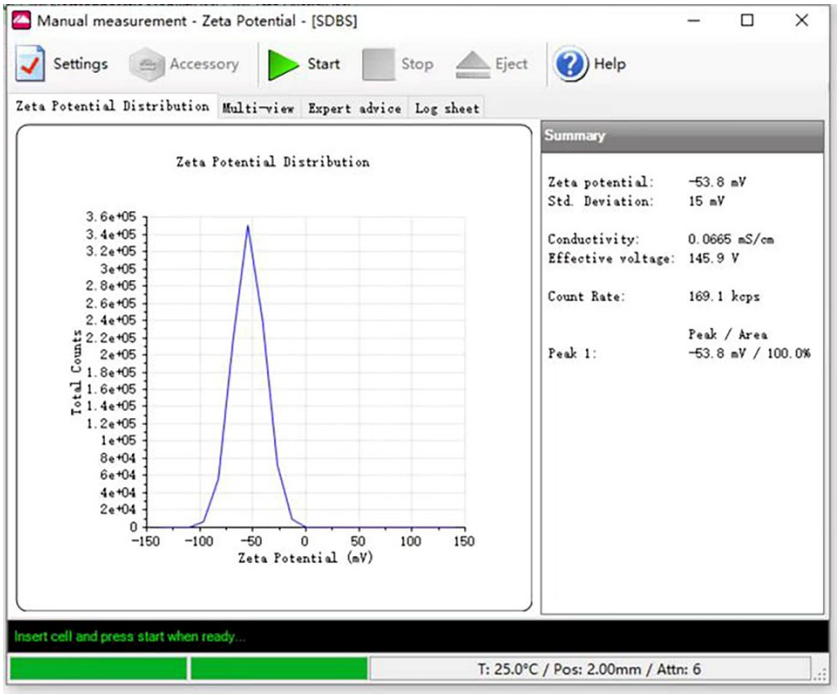

Figure S10. Zeta potential of **1** in water.

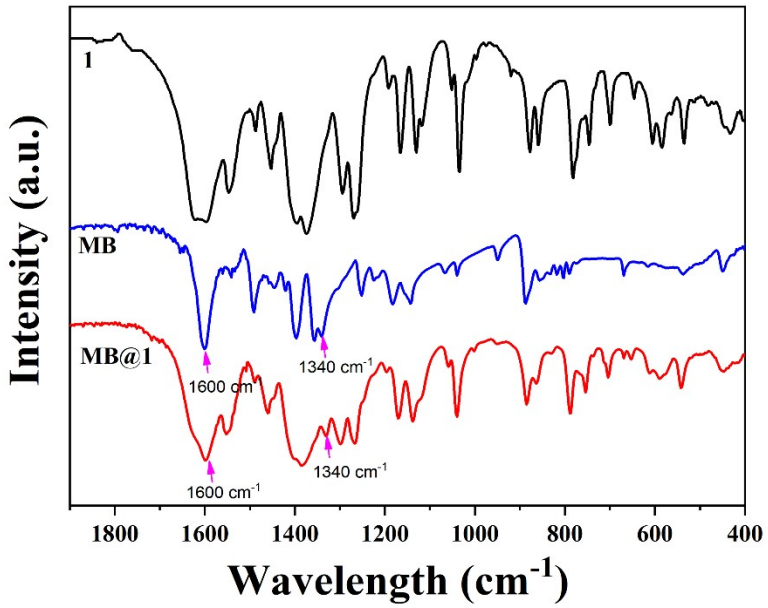
1
MB
MB@1
1600 cm-1
1340 cm-1
1600 cm-1
1340 cm-1
Intensity (a.u.)
1800
1600
1400
1200
1000
800
600
400
Wavelength (cm-1)

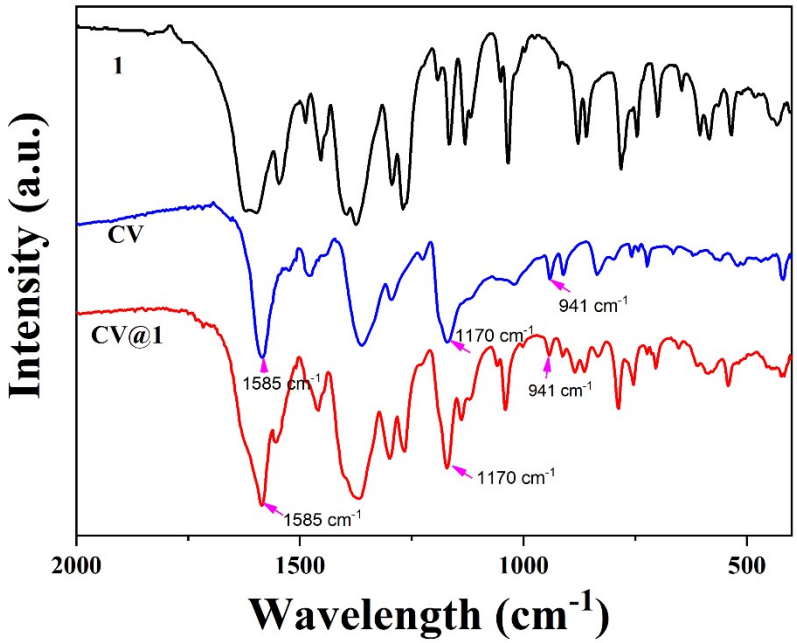
1
CV
CV@1
941 cm-1
1170 cm-1
1585 cm-1
941 cm-1
1170 cm-1
1585 cm-1
Intensity (a.u.)
2000
1500
1000
500
Wavelength (cm-1)

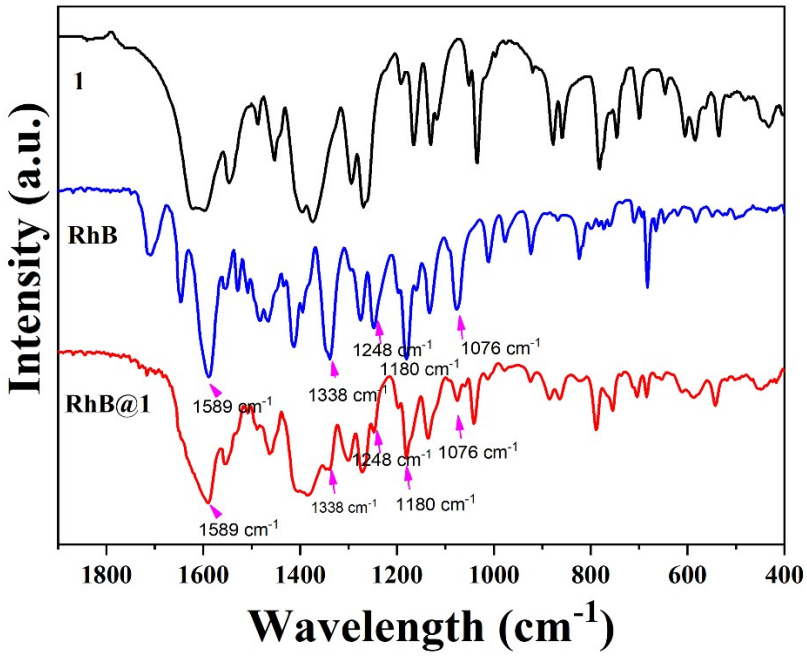

Figure S11. IR spectra of **1**, dyes and dye@**1**.

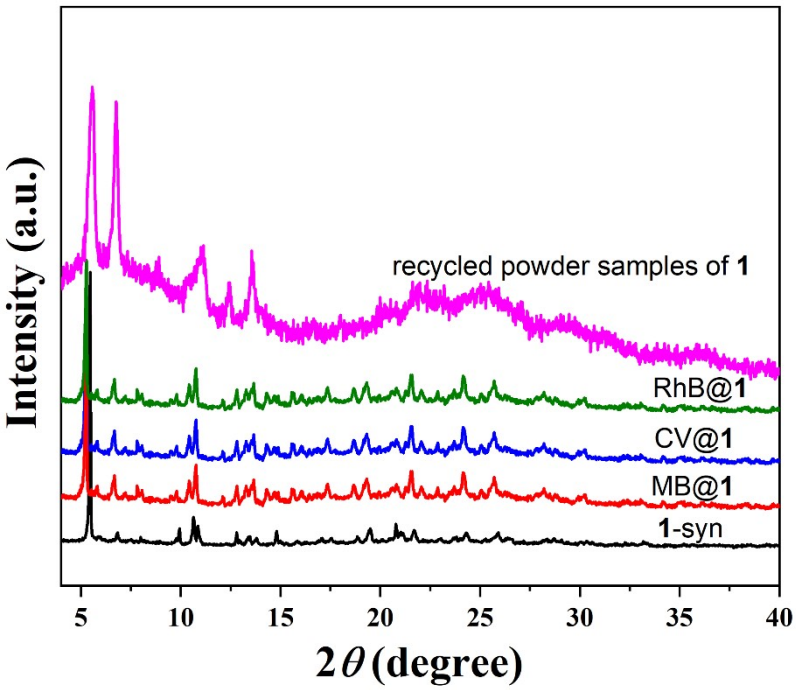

Figure S12. XRD patterns of crystal samples of **1** before and after dye adsorption.

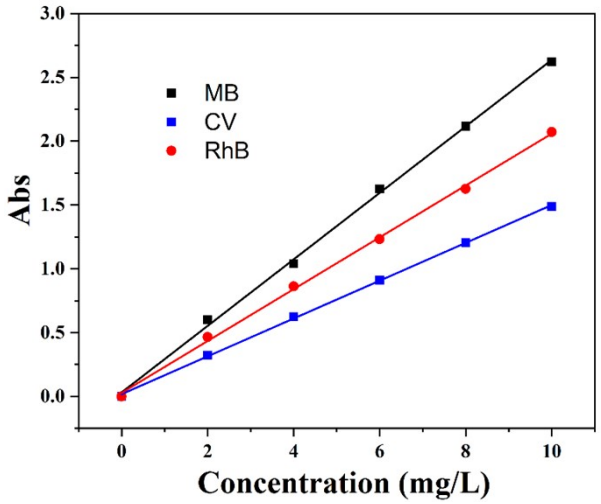

dyes	Fitting linear equations	R^2 (%)
MB	y = 0.2605 x + 0.03124	99.85
CV	y = 0.1482 x + 0.01771	99.94
RhB	y = 0.203 x + 0.028	99.85

Figure S13. The absorbed intensity (dots) of MB, CV and RhB at different concentrations (mg/L). The solid lines are the best linear fit.

Table S1. Equations for adsorption amounts and dye removal rate

Introduction	Equations	Comment
Adsorption amounts	$Q_t = \frac{(C_0 - C_t)V}{m}$	Where m (g) presents the weight of the adsorbent; C_0 (mg·L^{-1}) is the initial dye concentration and C_t (mg·L^{-1}) is the dye concentration at time t; V (L) denotes the volume of dye solution.
Dye removal rate (η, %)	$\eta = \frac{C_0 - C_t}{C_0} \times 100\%$	

Table S2. Adsorption kinetics model.

Introduction	Kinetic model	Comment
Pseudo first-order kinetics model	$ln(Q_e - Q_t) = lnQ_e - k_1 t$	Where Q_t and Q_e (mg·g^{-1}) are the adsorption capacity at time t and equilibrium; and k_1 (min^{-1}) is the pseudo-first-order rate constant.
Pseudo second-order kinetics model	$\frac{t}{Q_t} = \frac{1}{k_2 Q_e^2} + \frac{t}{Q_e}$	Where k_2 (g·mg^{-1}·min^{-1}) is the pseudo-second-order rate constant.

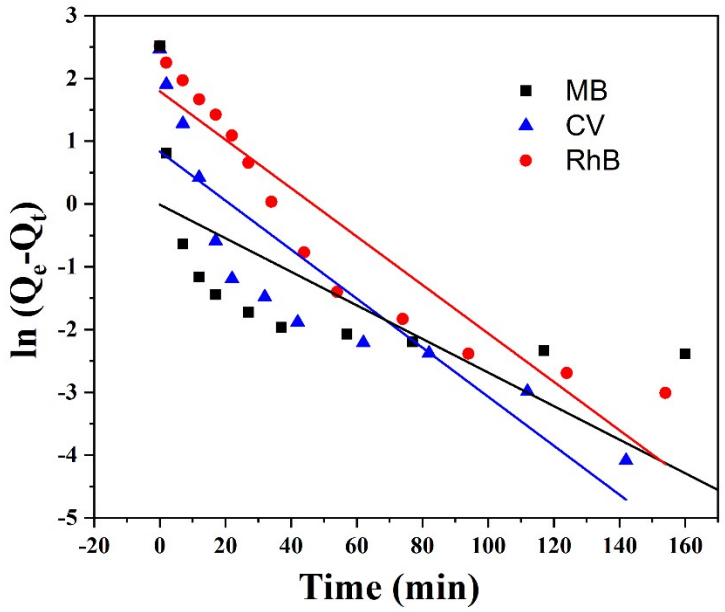

Figure S14. Plots of pseudo-first-order kinetics for the adsorption of MB, CV and RhB on **1** (Experiment Conditions: T = 25℃, V = 10 mL, C_0 = 10 mg·L^{-1}, m = 10 mg)

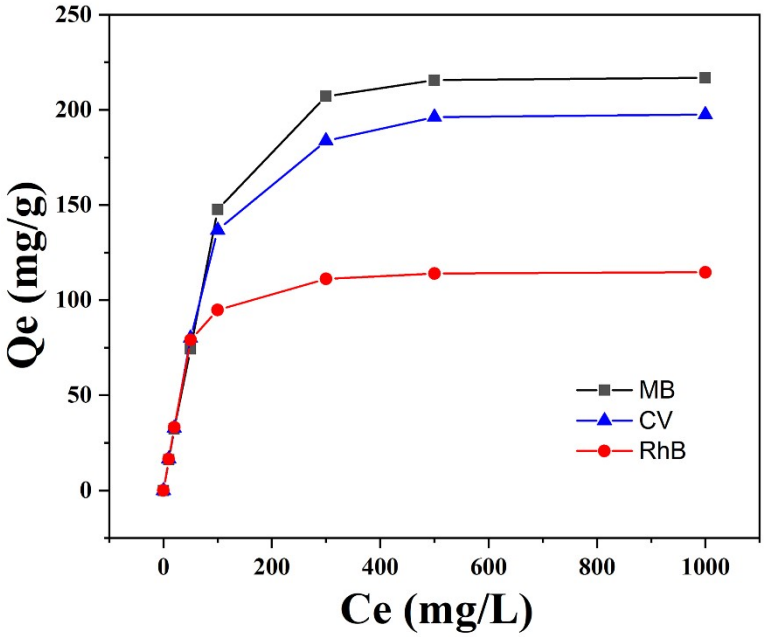

Figure S15. Adsorption isotherms of MB, CV and RhB on **1** at room temperature.

Table S3. Adsorption isotherm model

Introduction	Isotherm model	Comment
Langmuir isotherm	$\frac{C_e}{Q_e} = \frac{C_e}{Q_{max}} + \frac{1}{K_L q_{max}}$	Where C_e (mg L^{-1}) is the equilibrium concentration of adsorbate; Q_e and Q_m (mg L^{-1}) represent the equilibrium adsorption capacity and maximum adsorption capacity, respectively; K_L (mg L^{-1}) named the Langmuir constant;
Freundlich isotherm	$lnQ_e = lnK_F + \frac{1}{n}(lnC_e)$	Where K_F is the Freundlich constant related to the adsorption capacity; n is the adsorption strength constant under the Frundlich model.

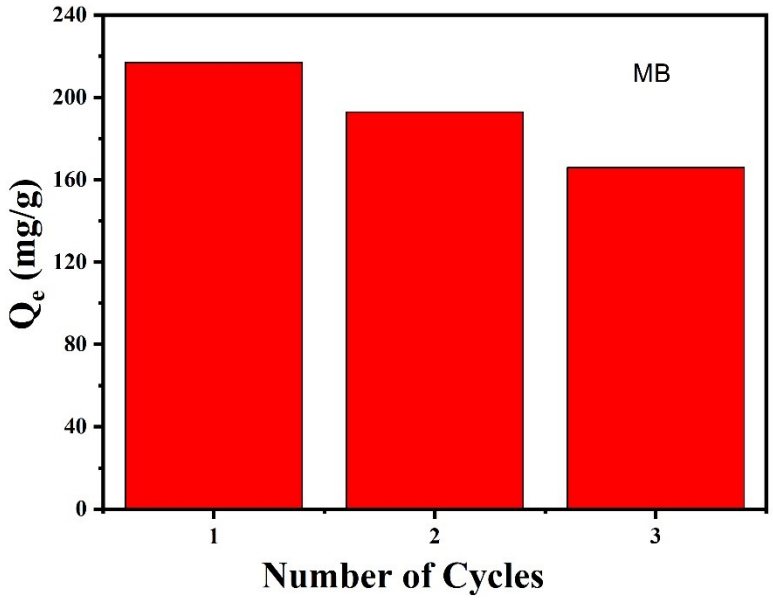

Figure S16. Reusability of **1** for the adsorption of MB.

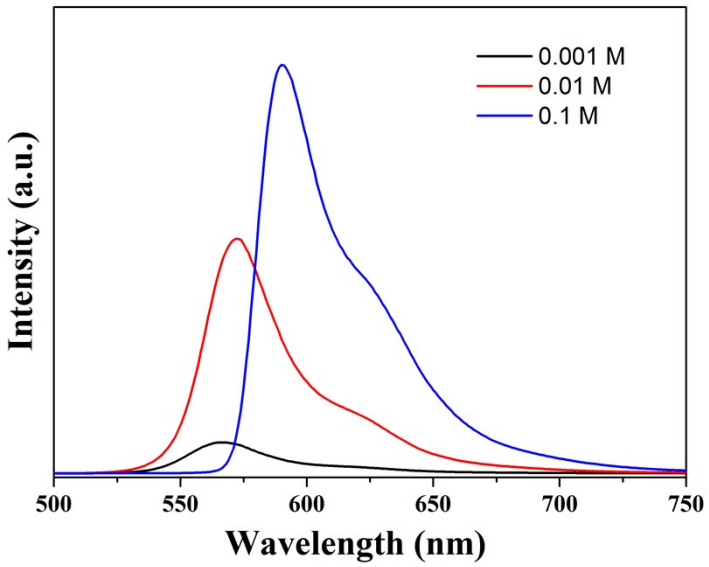

Figure S17. The fluorescent emission spectra of EtOH solution of RhB with different concentrations.

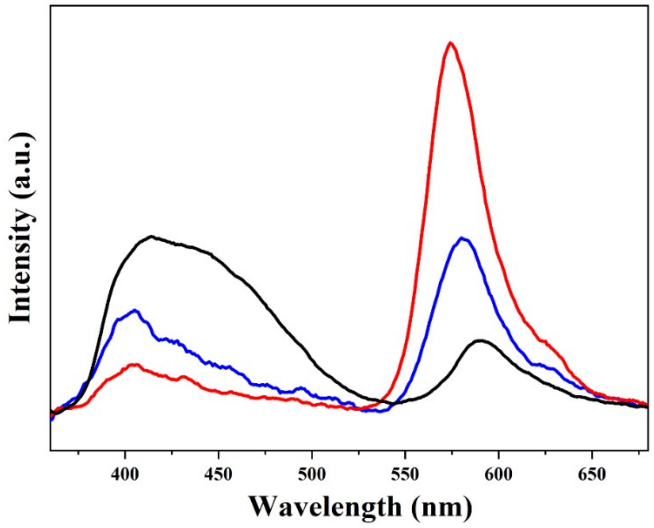

Figure S18. The fluorescent emission spectra of RhB@**1** in EtOH with different amounts of RhB.

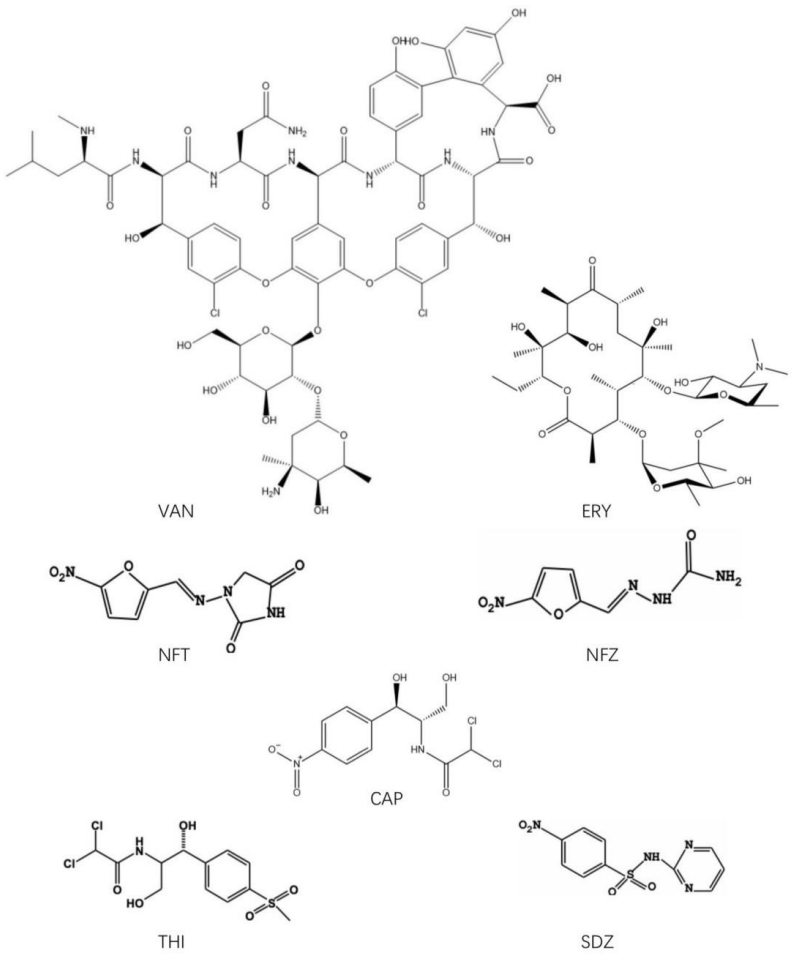

Figure S19. Molecule structures of the antibiotics selected in this work.

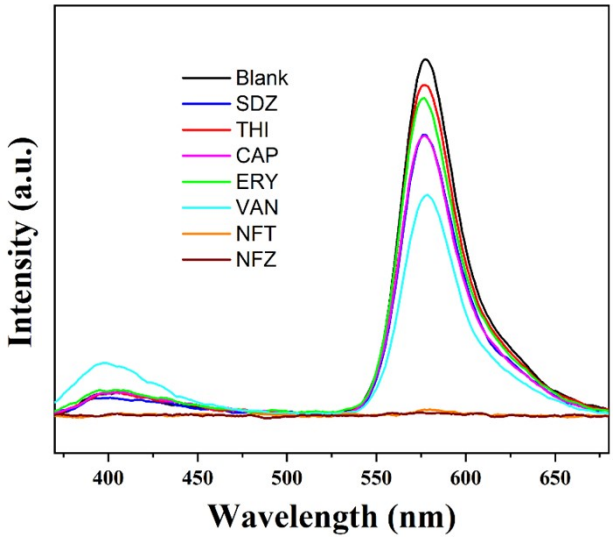

Figure S20. Fluorescence spectra of RhB@**1** dispersed into different antibiotics in EtOH solutions (700 μM).

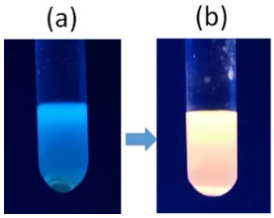

Figure S21. Color changes of **1** suspension upon RhB adsorption (a. **1** dispersed in EtOH; b. **RhB@1** dispersed in EtOH).

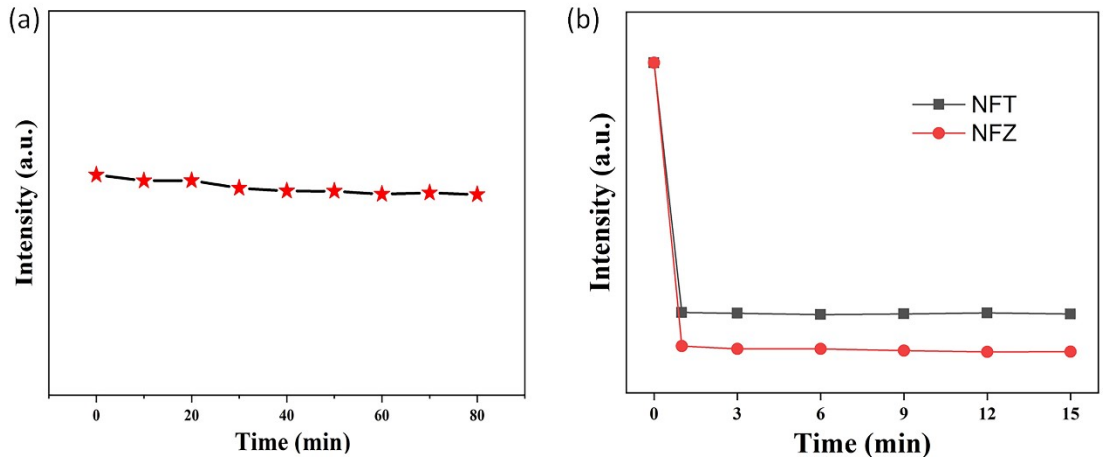

Figure S22. (a) Luminescent stability of suspension of **RhB@1** in EtOH within 80 minutes; (b) Response times of **RhB@ 1** towards NFT and NZF.

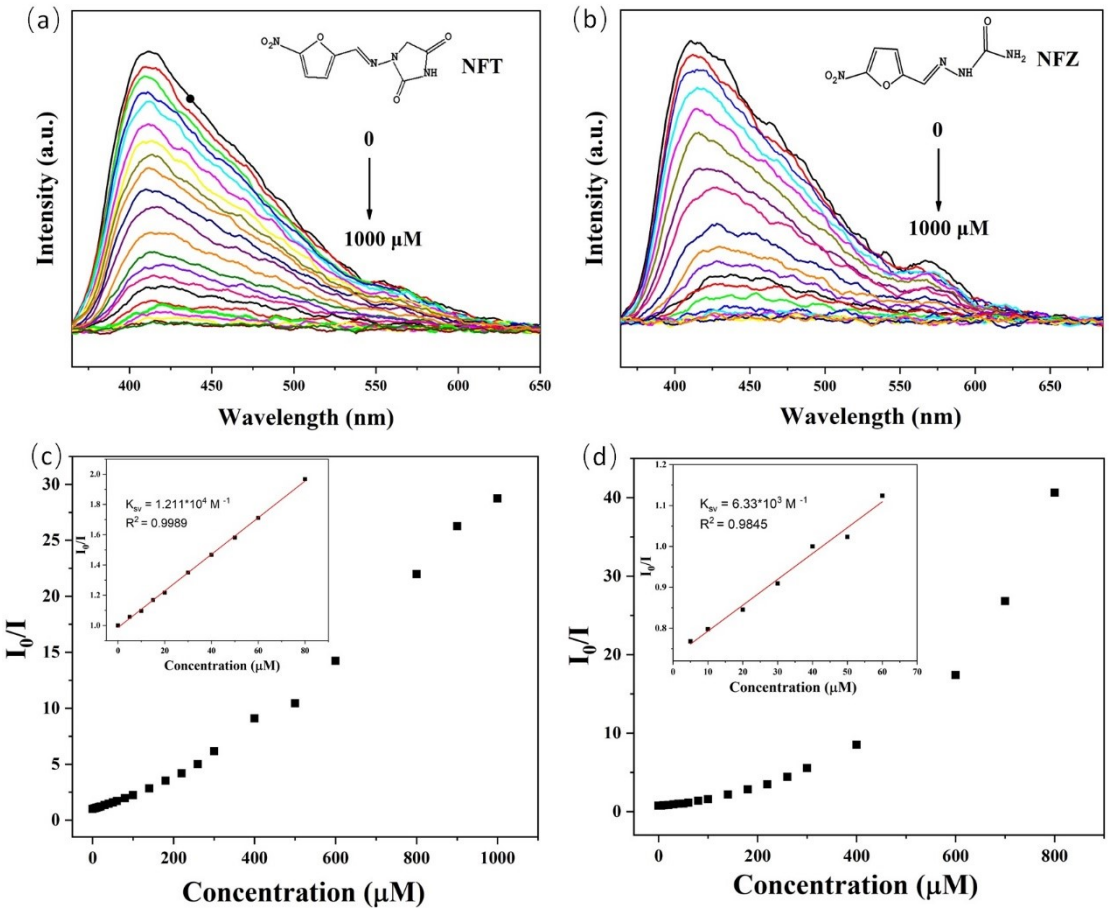

Figure S23. Emission spectra of **1** upon incremental addition of NFT (a) and NFZ (b); The Stern−Volume plots of **1** for NFT (c) and NFZ (d). Inset: Linear relationship of the SV plots at low concentration.

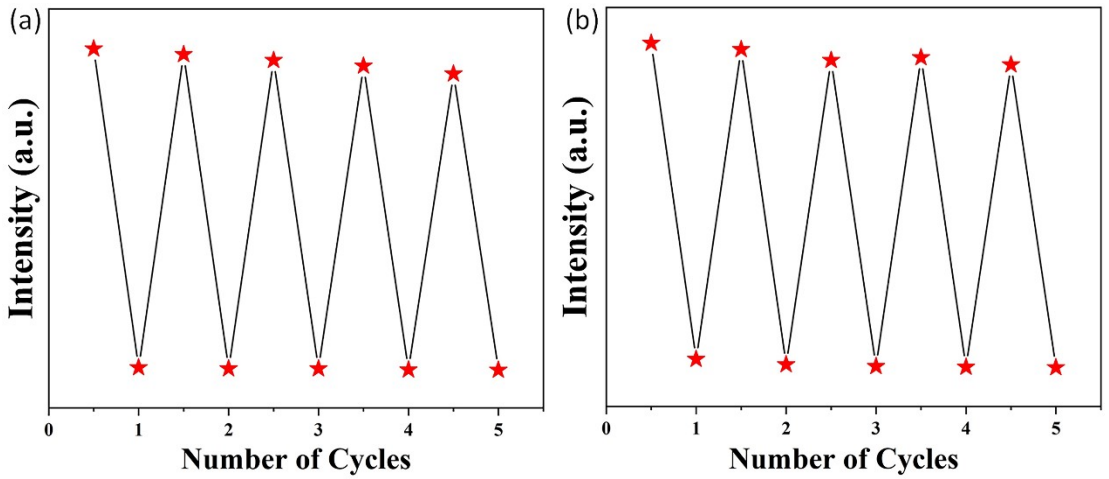

Figure S24. Fluorescence intensities of **1** in five recyclable experiments for sensing NFT (a) and NFZ (c) in EtOH.

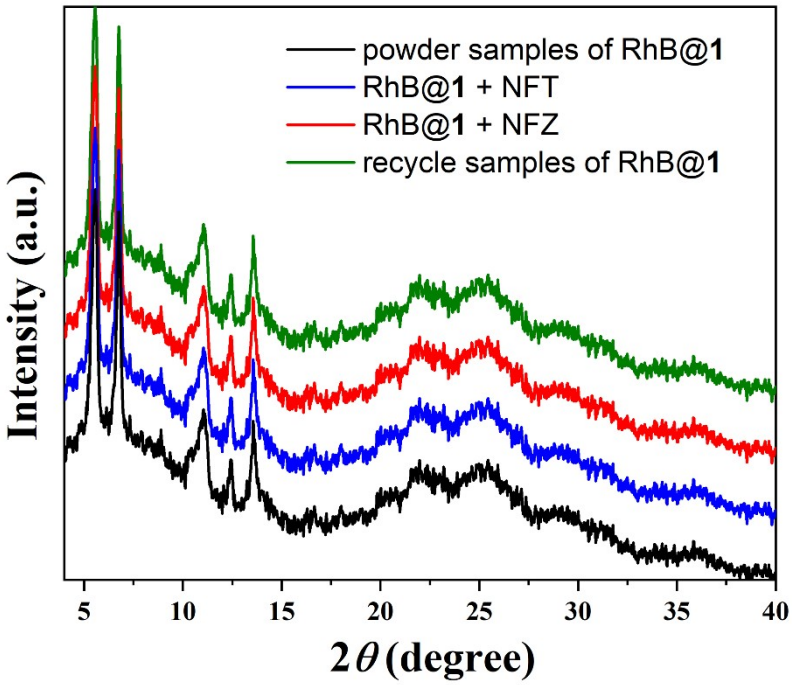

Figure S25. X-ray diffraction of RhB@**1** before and after sensing NFT/NZF.

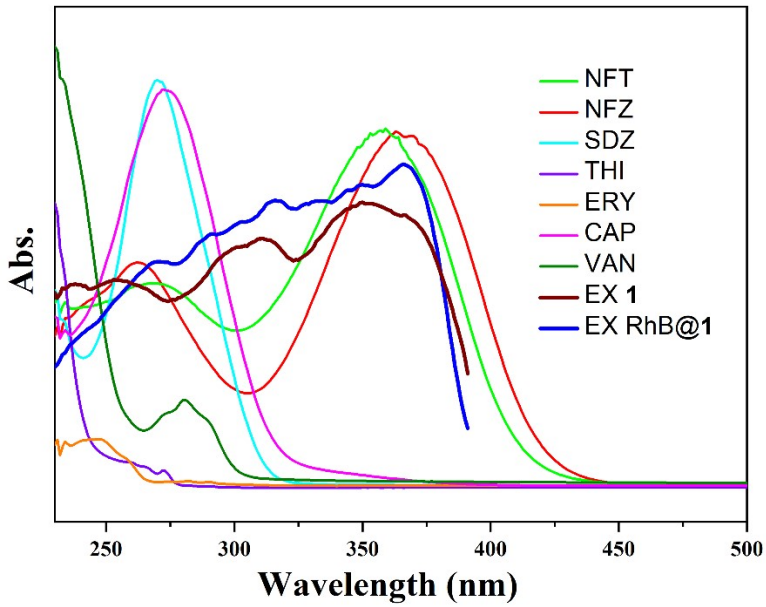

Figure S26. Spectral overlap between the absorption spectra of various antibiotics and the excitation spectrum of **RhB@1**.

Table S4. The values of K_{SV} and LOD of **RhB@ 1**, CP **1** and other reported MOF sensors towards NFT/NFZ.

MOFs	NFs	K_{SV} ($\times 10^4$ M^{-1})	LOD (μM)	solvent	Ref.
RhB@1	NFT	2.96	0.89	EtOH	This work
RhB@1	NFZ	2.08	0.98	EtOH	This work
CP 1	NFT	1.21	2.18	EtOH	This work
CP 1	NFZ	0.63	3.24	EtOH	This work
RhB@Zn-1	NFT	5.61	0.73	EtOH	1
RhB@Zn-1	NFZ	4.73	0.86	EtOH	1
$[Zn_2(Py_2TTz)_2(BDC)_2]\cdot 2DMF\cdot 0.5H_2O$	NFZ	1.726	0.91	H_2O	2
$[Eu_2(BCA)_3(H_2O)(DMF)_3]\cdot 0.5DMF\cdot H_2O$	NFT	1.6	0.16	H_2O	3
$[Eu_2(BCA)_3(H_2O)(DMF)_3]\cdot 0.5DMF\cdot H_2O$	NFZ	2.2	0.21	H_2O	3
$Zr_6O_4(OH)_8(H_2O)_4(CTTA)_{8/3}$	NFT	3.8	---	H_2O	4
$\{[Tb(TATMA)(H_2O)\cdot 2H_2O\}_n$	NFT	3.35	---	H_2O	5
$\{[Tb(TATMA)(H_2O)\cdot 2H_2O\}_n$	NFZ	3.00	---	H_2O	5
$[Cd_7(SO_4)_6(tppe)_2]$ 2DMF·$2H_2O$	NFZ	0.174	---	H_2O	6
$\{[NH_2(CH_3)_2]_4[Zn_3(HBDPO)_2(SO_4)_2]\}_n$	NFT	4.5	---	DMF	7

References:

1. Q.-Q. Tu, L.-L. Ren, A.-L. Cheng and E.-Q. Gao, *CrystEngComm*, 2021, **23**, 629-637.
2. Z.-W. Zhai, S.-H. Yang, M. Cao, L.-K. Li, C.-X. Du and S.-Q. Zang, *Cryst. Growth Des.*, 2018, **18**, 7173-7182.
3. F. Zhang, H. Yao, T. S. Chu, G. W. Zhang, Y. Wang and Y. Y. Yang, *Chem.-Eur. J.*, 2017, **23**, 10293-10300.
4. B. Wang, X.-L. Lv, D. Feng, L.-H. Xie, J. Zhang, M. Li, Y. Xie, J.-R. Li and H.-C. Zhou, *J. Am. Chem. Soc.*, 2016, **138**, 6204-6216.

5. Q.-Q. Zhu, H. He, Y. Yan, J. Yuan, D.-Q. Lu, D.-Y. Zhang, F. Sun and G. Zhu, *Inorg. Chem.*, 2019, **58**, 7746-7753.

6. Y. Zhao, Y.-J. Wang, N. Wang, P. Zheng, H.-R. Fu, M.-L. Han, L.-F. Ma and L.-Y. Wang, *Inorg. Chem.*, 2019, **58**, 12700-12706.

7. H. He, Q.-Q. Zhu, F. Sun and G. Zhu, *Cryst. Growth Des.*, 2018, **18**, 5573-5581.